ISSN (Print) : 0974-6846
Indian Journal of Science and Technology, *Vol 9(43), DOI: 10.17485/ijst/2016/v9i43/97000, November 2016* ISSN (Online) : 0974-5645

Modeling and Simulation of Gate Engineered Gate All-Around MOSFET for Bio-Molecule Detection

B. Padmanaban[1*], S. Sathiyamoorthy[1] and R. Ramesh[2]

[1]Department of Electronics and Instrumentation Engineering, JJ College of Engineering and Technology, Ammapettai, Poolangulathupatti (Post), Trichy - 620 009, Tamil Nadu, India; sbpnabhan@yahoo.co.in, sathyajayam@gmail.com
[2]Department of ECE, SASTRA University, Tirumalaisamudram, Thanjavur - 613 401,Tamil Nadu, India; ramesh24.dr@gmail.com

Abstract

Objectives: In this paper, modeling and simulation of a triple material gate stack gate all around MOSFET biosensor for the detection of biomolecules under dry environment conditions has been carried out. **Method:** A nanocavity is formed in the proposed device and its surface potential values are estimated by solving 2D Poisson and Schrödinger equations using Leibmann's iteration method. The surface potential values are obtained for both the presence and absence of biomolecules. To the best of our knowledge, the effect of engineering on the gate stack gate all around MOSFET biosensor characteristics has been studied for the first time and its characteristics such as sensitivity and drain current are obtained. **Findings:** It is found that the implementation of gate engineering in the gate stack gate all around MOSFET improves the characteristics of the device. **Improvements:** The proposed device may be improved by implementing the device as an optical biosensor for detection of biomolecules.

Keywords: Bio-Molecule Detection, Gate All Around MOSFET, Gate Engineering, Modelling, Simulation

1. Introduction

The design and fabrication of sensors for health care monitoring has drawn attention in the twenty first century. The development of micro- and nanoscale technologies proved to have a great potential for the development of next generation biosensors with increased sensitivity and reduced costs. FET based biosensors are portable and have an improved ability of detecting foreign and dangerous toxins. In the recent years, many types of FET biosensors have been developed and used in a wide variety of biomedical applications.

Nowadays for designing VLSI circuits the transistor size has to be scaled down. But as we reduce the channel length, the gate loses the control over channel and hence Short Channel Effects (SCE's) come into existence. SCE introduces the Drain Induced Barrier Lowering (DIBL), static power dissipation, gate oxide tunnelling leakage, sub-threshold voltage variation[1]. To overcome these effects multi-gate MOSFETs are used so that the gate acquires better control over channel and SCE's can be minimized[1]. Krishnaveni et.al.[2] has reported on a compact single MOSFET high voltage pulse generator. A high speed MOSFET for switching application is also reported for balance in channel and procedure of device design and fabrication for fast switching[3]. Saxena et.al.[4] have reported on the design of Voltage Controlled Oscillator (VCO) using FinFET and compared its performance with MOSFET VCO. Multigate MOSFETs can also be used for sensing of biomolecules. Various types of nanocavity embedded FET biosensor have been studied and reported. Multi-gate MOSFETs such as DG MOSFET and GAA MOSFET proved to have improved high frequency performance and low power operation. CMOS scaling also introduces a major limitation of SiO_2 gate dielectric thickness where it reached at the limit of few atomic

* *Author for correspondence*

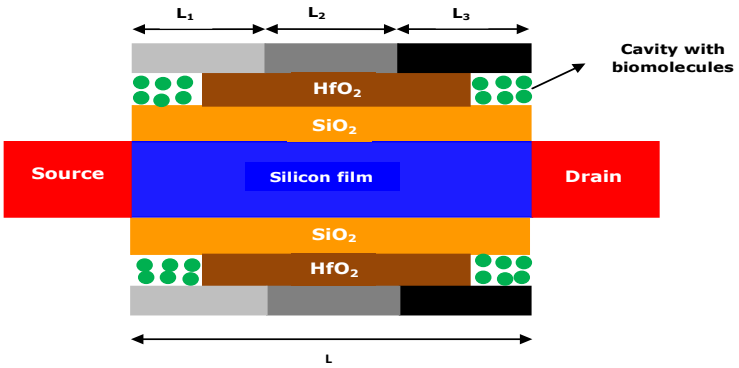

Figure 1. Cross-sectional view of a nanocavity embedded TMGSGAA MOSFET biosensor.

layers thickness. With this very small dielectric thickness, direct tunnelling of carriers takes place and increases the leakage current and degrades the circuit performance. To overcome this problem, high-k dielectrics are used, but it degrades the short channel performance of the device due to fringing field effects. These effects can be reduced by using gate stack architecture (high-k dielectric+SiO_2) and keeping EOT constant, reduces the direct tunnelling current[5].

A dielectric-modulated GAA MOSFET using vacuum as gate dielectric has been reported for detection of neutral and charged biomolecules[6] Narang et.al. have developed an analytical model for a dielectric modulated (DM) MOSFET for label free detection of biomolecules[7] An analytical model has been developed and reported for a four-gate dielectric modulated MOSFET biosensor for detection of biomolecules[8]. Narang et.al.[9,10] have reported an analytical model for a Tunnel Field-Effect Transistor (TFET) biosensor for detection of biomolecules. Dual Material Gate (DMG) or Tri-Material Gate (TMG) MOSFET uses two or three materials for the gate region. Gate material having higher work function is used near the source end (control gate) and a lower work function gate material is used near the drain end. This architecture prevents any changes in the drain bias (screening gate)[11,12]. It also changes the electrostatic potential profile to a step-like profile along the channel length due to the sudden increase of the electric field and electron velocity near the interface of the gate materials[13,14]. It also reduces the subthreshold leakage current and DIBL values and increases the output resistance and transconductance[15,16].

In this work, a 2D numerical modelling of TMGSGAA MOSFET biosensor has been developed and presented. Figure 1 shows the cross sectional view of TMGSGAA MOSFET Biosensor. The aim of this work is to obtain the electrostatic potential values by solving the 2D Poisson-Schrödinger equations self-consistently and simulate the other characteristics such as drain current and sensitivity of the device. The results are simulated for the presence and absence of bio-molecules in the nanocavity of the device.

2. Physics Based Modeling

The electrostatic surface potential of the channel region of TMGSGAA MOSFET is represented by 2-D Poisson's equation[17].

$$\frac{1}{r}\frac{\partial}{\partial r}\left(r\frac{\partial}{\partial r}u_k(r,x)\right)+\frac{\partial^2}{\partial x^2}u_k(r,x)=\frac{q[N_a(r,x)+n(r,x)+p(r,x)]}{\varepsilon_{si}} \quad (1)$$

$$k = 1,2,3$$

where $u_k(r,x)$ is the electrostatic potential value at a particular point along the position of channel length, N_a represents the acceptor concentration in the channel region, (x,r) is the direction along the channel length and perpendicular to the channel length. q is the electronic charge and ε_{si} is the silicon permittivity.

Region: I $0 \le x \le t_{si}$, $0 \le y \le L_{11}$

Region: II $0 \le x \le t_{si}$, $L_{11} \le y \le L_{11}+L_{12}$

Region: III $0 \le x \le t_{si}$, $L_{11}+L_{12} \le y \le L_{11}+L_{12}+L_{13}$

$n(r,x)$ and $p(r,x)$ are the electron and hole concentrations of the device, $k = 1,2,3$ represent the regions for metal gate 1 (M_1), metal gate 2 (M_2) and metal gate 3 (M3) respectively. The flat band voltage of the device is calculated using the metal gate work functions

$$V_{FBi} = \emptyset_{mi} - \emptyset_{s,} \quad i = 1,2,3 \tag{2}$$

$\emptyset_s$ - silicon work function[17].

$$\emptyset_s = \chi_s + \frac{E_g}{2q} + \emptyset_F \tag{3}$$

where $\emptyset_F$ is the Fermi potential and is given by[17].

$$\emptyset_F = \frac{KT}{q} ln\left(\frac{N_a}{n_i}\right) = V_T ln\left(\frac{N_a}{n_i}\right) \tag{4}$$

E_g is the silicon bandgap, χ_s is the electron affinity, V_T is the thermal voltage, n_i is the intrinsic carrier concentration and K is the Boltzmann constant.

The 2-D Poisson equation is solved using the boundary conditions.

$$C_{ox}\left[V_{g1}^{*} - \emptyset_{m1} - U_k(r,x)\right] = \varepsilon_{si}\frac{\partial U_k(r,x)}{\partial r}\Big|r = \frac{t_{si}}{2}$$

$$0 < x < L_1$$

$$C_{ox}\left[V_{g2}^{*} - \emptyset_{m2} - U_k(r,x)\right] = \varepsilon_{si}\frac{\partial U_k(r,x)}{\partial r}\Big|r = \frac{t_{si}}{2},$$

$$L_1 < x < L_1 + L_2$$

$$C_{ox}\left[V_{g3}^{*} - \emptyset_{m3} - U_k(r,x)\right] = \varepsilon_{si}\frac{\partial U_k(r,x)}{\partial r}\Big|r = \frac{t_{si}}{2},$$

$$L_1 + L_2 < x < L_1 + L_2 + L_3 \tag{5}$$

At the source channel junction the electrostatic potential is the built-in potential for that junction. The built-in potential at the drain side is increased by the drain voltage V_{ds}[17].

$$U(x = 0) = V_{bi} \quad U(x = L) = V_{bi} + V_{ds} \tag{6}$$

where

$$L = L_1 + L_2 + L_3$$

and

C_{ox} is the total oxide capacitance per unit area including the high-k and SiO_2 layer[17].

$$C_{ox} = {\varepsilon_{ox}}/{t_{oxeff}} \tag{7}$$

t_{oxeff} is the effective oxide thickness (SiO_2+HfO_2)[17].

The effective oxide thickness varies for L_{11}, L_{12}, L_{13}. Accordingly, we have calculated the t_{oxeff} values for different regions.

$$t_{oxeff} = t_1 + t_2\frac{\varepsilon_1}{\varepsilon_2} \tag{8}$$

t_1 is SiO_2 thickness, t_2 is the high-k layer thickness, ε_1 is the permittivity of SiO_2 and ε_2 is the permittivity of HfO_2.

$$V_g^{*} = V_{g1}^{*} + V_{g2}^{*} + V_{g3}^{*} \tag{9}$$

is the effective gate voltage and represented as $V_{g1}^{*} = V_{gs} - V_{FB1}$; $V_{g2}^{*} = V_{gs} - V_{FB2}$ and

$V_{g3}^{*} = V_{gs} - V_{FB3}$ where $V_{FB1}, V_{FB2}, V_{FB3}$ are the flat-band voltages.

The 2D effective mass Schrödinger equation along the n-channel is given by

$$-\frac{\hbar^2}{2m_x^{*}}\nabla^2\Psi_0(r,x) + qU_k(r,x)\Psi_0(r,x) = E_0\Psi_0(r,x) \tag{10}$$

The 2-D Schrödinger equation (10) is reduced to 1-D Schrödinger equation using variable separation method[17] [13]

$$\frac{-\hbar^2}{m_x^{*}}\frac{\partial^2\Psi_0(r)}{\partial r^2} + (-q)U_k(r)\Psi_0(r) = E_0\Psi_0(r) \tag{11}$$

where $m_x^{*} = 0.916m_0$ is the effective mass of electrons in the lowest energy level with <100> orientation, E_0 is the lowest sub-band energy, ħ is the reduced Planck's constant and $u_k(r,x)$ is the value of surface potential. $\Psi_0(r)$ is the trial wave function[17].

The drain current I_D is expressed as[17].

$$I_D = \mu_{eff}\left(\frac{2\pi r}{L}\right)C_{ox}(V_T)^2[f(Q_d) - f(Q_s)] \tag{12}$$

Where $f(Q_d)$ and $f(Q_s)$ are written as:

$$f(Q_{in}) = -V_T Q_{in} - \frac{R}{2\varepsilon_{si}}\frac{Q_{in}^2}{2} - \frac{Q_{in}^2}{2C_{ox}} \tag{13}$$

Q_d and Q_s are obtained by evaluating Q_{in} at source (V=0) and at drain (V=V_{ds}).

The effective mobility is obtained from the equation (14).

$$\mu_{eff} = \frac{\mu_1}{1 + \theta_i\left(V_{gs} - V_{th}\right)\left(1 + \frac{\mu_1}{V_{sat}}\frac{V_{ds}}{L}\right)} \tag{14}$$

$\theta_i = 0.6$ is the fitting parameter associated with mobility reduction due to surface roughness scattering, V_{th} is calculated as given in:

$$\mu_1 = \frac{\mu_0}{\sqrt{1 + \left[N_a \Big/ \left(N_{ref} + \left(N_a / S \right) \right) \right]}} \quad (15)$$

where μ_0 is electron mobility with its value taken to be677 $cm^2/V\,s$, the values of the parameters S= 350, $N_{ref} = 3 \times 10^{22}\ m^{-3}$and high field saturation velocity $V_{sat} = 10^7$ cm/s.

The sensitivity of the device is calculated using[18].

$$S = \frac{\Delta I_d}{\Delta u_k(r,x)} \quad (16)$$

3. Computational Technique

The 2D Poisson's Eqn. (1) is solved numerically using Leibmann's iterative method and the electrostatic surface potential values are obtained V_{gs} and V_{ds} values. The electrostatic potential are then substituted to 1D Schrödinger equation. It is then solved numerically using Leibmann's iteration method using the boundary conditions and the exact value of surface potential is obtained. Table 1 shows the parameters and constants used in the simulation of biosensor.

$$u_k(i,j+1) = i^2 h^2 \frac{qN_a}{\varepsilon_s} + (4+i)u_k(i,j) - (1+i)u_k(i+1,j) - u_k(i-1,j) + u_k(i,j-1)$$

For $i = 1,2,3,\ldots.$ and $j = 1,2,3,\ldots.$ (17)

The other characteristics of the device such as drain current, sensitivity are then estimated.

3.1 Algorithm

Step 1. Assign gate length, channel length, device width, height and thickness of silicon fin.
Step 2. Apply bias voltages.
Step 3. Start with a trial potential $U_k(r,z)$. Obtain the electron concentration n(r,z).
Step 4. Determine numerically the surface potential by solving the 3D Poisson's equation using Leibmann's iteration method by applying appropriate boundary conditions for 20x20 iterations.
Step 5. Substitute this surface potential value in the 1-D Schrödinger's equation.
Step 6. Solve the 1-D Schrödinger's equation using Leibmann's iteration method.
Step 7. Calculate new n(r,z) value from the obtained wave functions and their corresponding Eigen energies.
Step 8. A new surface potential value $U_k(r, z)$ is obtained.
Step 9. Calculate the relative error of the surface potential between the exact and simulated values.
Step 10. Repeat step 4 to step 9 until it converges (error<0.0001) by increasing the number of iterations.
Step 11. Estimate the exact value of surface potential at every point along the channel length.
Step 12. Obtain the other characteristics of the device.

4. Results and Discussion

Table 1. Parameters and constants[17].

Parameters	Values
Gate Length (L_g)	36nm
Silicon film thickness (t_{si})	20nm
Channel Length (L_{eff})	36nm
Intrinsic carrier concentration (n_i)	$10^{10}/cm^3$
Acceptor concentration (N_a)	$10^{16}/cm^3$
Donor Concentration (N_D)	$10^{20}/cm^3$
Built-in potential (V_{bi})	0.55V
Thickness of SiO_2	1nm
Thickness of high-k dielectric	1.5nm

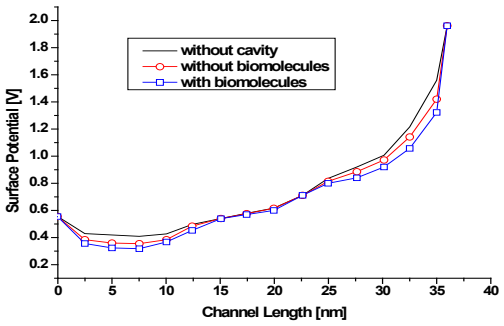

Figure 2. Surface potential variation along channel length for Vds = 1V.

Figure 2 shows the electrostatic potential variation of the TMGSGAA MOSFET sensor for the presence and absence of biomolecules. It is found that the surface potential values are less pronounced for the presence of biomolecules than for its absence due to the variation of the dielectric constant (k) of the device. When the target biomolecules are absent in the nanogap cavities,

air gets filled and the threshold voltage values will move in the positive direction. This is due to the change in the dielectric constant (K) of the device. When the target biomolecules are present in the sensing region, the dielectric constant will be changed from to higher values and the device electrical characteristics will also change.

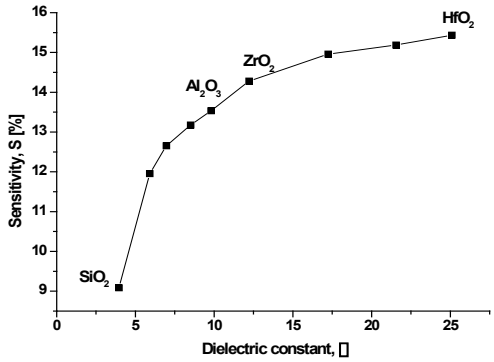

Figure 3. Simulated sensitivity Vs Dielectric constant for Vds = 1V.

Figure 3 shows the sensitivity variation of the device for different dielectric values ε of 3.9, 10,13,25. These values correspond to SiO_2, Al_2O_3, ZrO_2 and HfO_2. It is found that the sensitivity of the TMGSGAA MOSFET biosensor is high for HfO_2 compared to other dielectric constants. The gate voltage (V_{gs}) varies between -0.75V to 1.5V.

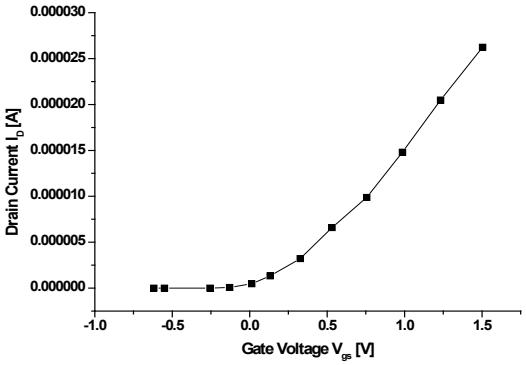

Figure 4. Drain Current variation with respect to the gate voltage.

Figure 4 shows the drain current variation of the device for the variation in the gate voltage V_{gs} for a fixed value of drain voltage V_{ds}=1V. It produces a maximum current at V_{gs}=1.5V and found that the current increases as the V_{gs} values are increased. The variation of sensitivity of the TMGSGAA MOSFET sensor with respect to the variation in gate voltage V_{gs} is shown in Figure 5. The sensitivity is maximum at V_{gs}=-0.6V.

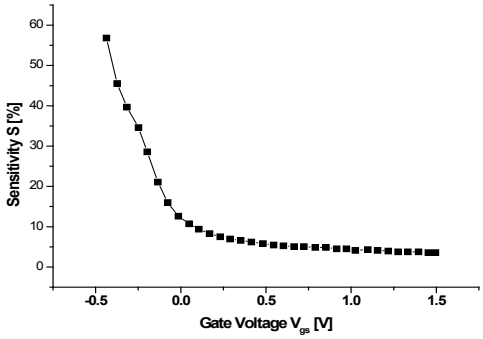

Figure 5. Sensitivity variation Vs gate voltage Vgs for Vds=1V.

5. Conclusion

The 3-D numerical modeling of TMGSGAA MOSFET biosensor using HfO_2 for determination of biomolecules has been developed. The self-consistent solution of the 3D Poisson-Schrödinger equations has been used for modeling of the device. It is found that using HfO_2 as oxide material in gate engineered gate stack gate all around devices increase its sensivity. It is also found that the device is suitable for biosensing applications.

6. References

1. Krishnaveni S, Rajini V. Implementation of an Economical and Compact Single MOSFET High Voltage Pulse Generator, Indian Journal of Science and Technology. 2015 Aug; 8(17). Doi:10.17485/ijst/2015/v8i17/62205
2. Hamed Sepahv, Soghra Raisi. A High Speed MOSFET for Switching Application, Indian Journal of Science and Technology. 2015 Sep; 8(22). Doi: 10.17485/ijst/2015/v8i22/61332
3. Siddharth Saxena, Srikanth M, Shantanu Jawale, Sakthivel R. Efficient VCO Using FinFET, Indian Journal of Science and Technology. 2015 Jan; 8(S2). Doi: 10.17485/ijst/2015/v8iS2/67807.
4. Deshpande Akshay, Sanidhya Mohan Sharma, Lochan Anil Vyas, Sivasankaran K. Design of Low Power and Area Effi-

cient 4-bit Arithmetic and Logic Unit using Nanoscale FinFET, Indian Journal of Science and Technology. 2015 Jan; 8(S2). Doi: 10.17485/ijst/2015/v8iS2/70759.
5. Pradhan K, Mohapatra S, Sahu P, Behera D. Impact of High-K Gate Dielectric on Analog and RF Performance of Nanoscale DG-MOSFET, Microelectronics Journal, 2014; 45(2):144-51.
6. Gautam R, Saxena M, Gupta R, Gupta M. Numerical Model of Gate-All-Around MOSFET with Vacuum Gate Dielectric for Biomolecule Detection, Electron Device Letters, IEEE. 2012; 33(12):1756-58.
7. Narang R, Saxena M, Gupta M. Analytical Modeling of a Split-Gate Dielectric Modulated Metal-Oxide-Semiconductor Field-Effect Transistor for Application as a Biosensor, In: Devices, Circuits and Systems (ICDCS), 2nd International Conference on, IEEE, Combiatore, 2014, p. 1-6.
8. Narang R, Saxena M, Gupta M. Drain Current Model of a Four-Gate Dielectric Modulated MOSFET for Application as a Biosensor, Electron Devices, IEEE Transactions. 2015; 62(8):2636-44.
9. Narang R, Reddy KS, Saxena M, Gupta R, Gupta M. A Dielectric-Modulated Tunnel-FET-Based Biosensor for Label-Free Detection: Analytical Modeling Study and Sensitivity Analysis, Electron Devices, IEEE Transactions. 2012; 59(10):2809-17.
10. Narang R, Saxena M, Gupta R, Gupta M. Dielectric Modulated Tunnel Field-Effect Transistor-A Biomolecule Sensor, Electron Device Letters, IEEE. 2012; 33(2):266-68.
11. Pal A, Sarkar A. Analytical Study of Dual Material Surrounding Gate MOSFET to Suppress Short-Channel Effects (SCEs), Engineering Science and Technology, International Journal. 2014; 17(4):205-12.
12. Arefinia Z, Orouji AA. Quantum Simulation Study of Dual-Material Double Gate (DMDG) MOSFET: NEGF Approach, In: IEEE Silicon Nanoelectronics Workshop, HI, 2008, p. 1.
13. Ramya MA, Nirmal D, Soman S, Nair PP, Jeba IK. Analysis of Gate Engineered SOI MOSFET for VLSI Application, In: Automation, Computing, Communication, Control and Compressed Sensing (iMac4s), International Multi-Conference on, IEEE, Kottayam, 2013, p. 498-501.
14. Vishnoi R, Kumar MJ. Compact Analytical Model of Dual Material Gate Tunneling Field-Effect Transistor using Interband Tunneling and Channel Transport, Electron Devices, IEEE Transactions. 2014; 61(6):1936-42.
15. Razavi P, Orouji AA. Dual Material Gate Oxide Stack Symmetric Double Gate MOSFET: Improving Short Channel Effects of Nanoscale Double Gate MOSFET, In: Electronics Conference, BEC 11th International Biennial Baltic, IEEE, Tallinn, 2008, p. 83-6.
16. Ghosh P, Haldar S, Gupta R, Gupta M. An Analytical Drain Current Model for Dual Material Engineered Cylindrical/Surrounded Gate MOSFET, Microelectronics Journal. 2012; 43(1):17-24.
17. Padmanaban B, Ramesh R, Nirmal D, Sathiyamoorthy S. Numerical Modeling of Triple Material Gate Stack Gate All-Around (TMGSGAA) MOSFET Considering Quantum Mechanical Effects, Superlattices and Microstructures. 2015; 82:40-54.
18. Rigante S, Lattanzio L, Ionescu AM. FinFET for High Sensitivity Ion and Biological Sensing Applications, Microelectronic Engineering. 2011; 88(8):1864--66